Experimental Investigations on a Heteropolar Electrodynamic Bearing-self-bearing Motor

Virginie Kluyskens [a], Joachim Van Verdeghem[a], Corentin Dumont, Bruno Dehez [a]

[a] Center for Research in Mechatronics (CEREM), Institute of Mechanics, Materials and Civil Engineering (IMMC), Université catholique de Louvain (UCL), Louvain-la-Neuve 1348, Belgium, virginie.kluyskens@uclouvain.be

***Abstract*—This article describes how multifunction windings can passively generate electrodynamic centering forces and when fed by a power supply, a driving torque. It shows the experimental EMF measures, both for the electrodynamic centering and for the motor functions, obtained on a prototype, operating in quasi-static conditions. It also shows the measured radial forces and the measured torque in these conditions.**

I. INTRODUCTION

Self-bearing motors are an attractive solution to respond to issues related to compactness and maximum spin speed. A lot of types of electrical motors have been studied for self-bearing operation, where self-bearing operation means a system in which the drive function and the bearing function are magnetically integrated. This bearing function is always realized with the principle of magnetic bearings in which the generation of the guidance forces is controlled by modulating a current as a function of the rotor position. Active guidance in self-bearing-motor can be related to active magnetic bearings (AMBs), which allow reaching relatively high stiffness values, high positioning precision, and have reached a certain level of industrial maturity. However, the complexity, cost and overall dimensions associated with this control system can be prohibitive, e.g. for small rated power applications.

Passive guidance for self-bearing motors has not been investigated much yet. However, some references show that when short-circuiting the guidance windings of self-bearing motors, some restoring forces appear. [1] shows a self-bearing induction motor with the rotor mounted on a flexible shaft and supported by external bearings. The bearing windings, usually controlled to provide an active guidance for the rotor, were simply short-circuited. The article shows that the vibrations decreased with short-circuited bearing windings compared with open circuit bearing windings, but less than when the bearing windings are actively controlled. The same kind of observation was reported in [2] for a two-pole induction motor. Finally, the principle of radial forces generation with bearing windings in short circuit for a self-bearing switched reluctance machine is studied in [3] and here also a decrease in the vibrations was observed.

This passive guidance could be improved if those short-circuited bearing windings were designed and optimized for passive guidance. This is the case of electrodynamic magnetic bearings (EDB). EDB generate guiding forces by the interaction of a permanent magnetic field and currents induced by the motion of this magnetic field. Usually EDB are designed to be null-flux bearings, which means that there are no currents induced when the moving part is at its equilibrium position. However, these bearings are difficult to design as their stability depends on the rotor spin speed and on the damping present in the system [4]. Moreover, their stiffness depends on the spin speed, and the specific load capacity of EDB remains lower than AMB's [5].

Centering homopolar EDB have focused much interest, resulting in dynamical models [4,6], prototypes and a successful levitation test [7]. More recently, centering heteropolar bearings have been studied, leading to design rules on the windings so as to be null-flux [8], and to a model predicting the dynamical behavior and forces generated in those kind of bearings [9]. Heteropolar EDB present a structure close to permanent magnet (PM) motors, and an integration of the EDB inside the PM motor gives the opportunity to exploit the magnetic field produced by the permanent magnets already present inside the motor also for the generation of radial forces. It can also be noted that PM motors are particularly well suited for high spin speed operation and that EDB produce a maximal stiffness at high spin speed, which gives even more sense to this integration. This kind of integration, a centering heteropolar EDB inside a PM motor, has already been described in [10], for two cases: the first one with two distinct windings systems for the motor and the guidance functions, and the second one with one single multifunction winding system. A FE study of an application case is also considered in this paper, showing the theoretical feasibility of such a device, for a slotless winding configuration.

The goal of this paper is to go a step further in the study of self-bearing PM motors, in which the passive electrodynamic guidance generation takes place in the same winding as the torque generation of the motor. A prototype of a heteropolar centering EDB with a radial magnetic field has been constructed, and its guidance performances have been studied in [11]. Consecutive to the theoretical studies presented in [10], this prototype is investigated as a self-bearing motor in this article, to confirm its ability to also develop a driving torque. The present article first briefly explains how a single winding can be designed to act as an EDB winding and as a motor winding. In the next section, the prototype and the test bench are described. Finally, the article shows quasi-static experimental results, in terms of electromotive force (EMF), both for the EDB and for the motor functions, and in terms of radial forces and of torque.

II. OPERATING PRINCIPLE

This section briefly describes the general operating principle of a single winding performing both drive and EDB

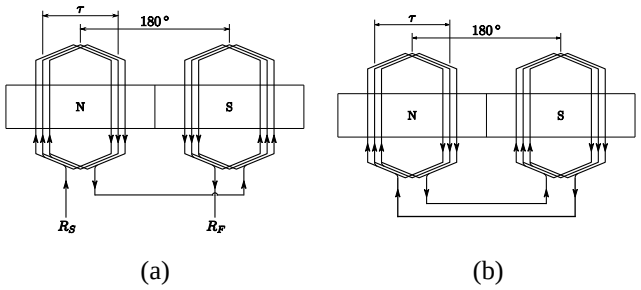

Figure 2. Unrolled view of one phase (a) of a motor winding and (b) for an electrodynamic bearing winding,both in the case of a one pole pair internal permanent magnet rotor.

bearing principle, in the case of a one pole pair PM rotor. In the case of a one pole pair rotor (p=1), the motor winding also has one pole pair to be magnetically coupled to the rotor, and to produce a torque. An example of such a winding is shown

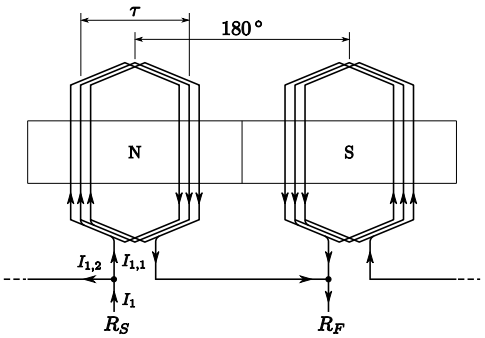

Figure 3. Unrolled view of phase 1 of a multifunction winding, performing both motor and passive EDB centering functions, for a one pole pair internal permanent magnet rotor.

in Fig. 1(a). As for the EDB winding, as explained in [6], when the rotor is an internal rotor, the EDB short-circuited bearing winding has to have two pole pairs (p+1), to be magnetically coupled to the harmonics linked to the rotor off-centering. An example of such a winding is shown in Fig. 1(b).

These two windings can be combined into one single multifunction winding, as shown in Fig. 2 for one phase. This winding can be fed through terminals R_S and R_F to produce a torque: both coils are then connected in anti-parallel. But this winding also allows for a short circuit path, this path consisting of both coils connected in series. The currents induced when the rotor is moving out-centered can then circulate in this short-circuit path and generate electrodynamic restoring forces.

III. BASIC MODEL

Let us assume the following hypothesis:

- the materials have linear magnetic characteristics,
- only the highest harmonics in the permanent magnet field distribution are considered,
- the rotor only undergoes translational eccentricity, i.e. the magnetic axis of the rotor and of the winding remain parallel,
- the rotor spin speed is constant.

Based on these assumptions, the magnetic vector potential due to the permanent magnet rotor is axial and can be derived as in [6] and [7]. Finally, when the rotor is internal and has one pole pair, the magnetic vector potential is worth at a point *P* placed at *(r, θ)* from the stator center, see Fig. 3:

$$A_{Mz}(r,\theta) = A(r)\sin(\theta - \omega t) + \epsilon A^i(r)\sin(2\theta - \omega t - \phi) \quad (1)$$

where *A(r)* and $A^i(r)$ are the amplitude of the vector potential component of periodicity *p=1* when the rotor is centered and of periodicity *p+1=2* when the rotor is off-centered respectively. They depend on the geometric and magnetic properties of the system. The distance between the rotor and stator center is named ε, and the direction of off-centering is named ϕ.

Considering window frame windings connected as illustrated on Fig. 2 and considering (1), the magnetic flux seen by each coil of the winding of phase *k* can be calculated by integrating $\Phi = \oint_{\Gamma_k} \vec{A}\vec{dl}$, along the conductors of these coils. And from there the electromotive forces *E* generated on each coil is calculated by derivation of the flux $E = -\frac{d\Phi}{dt}$, as detailed in [8].

$$E_0 = \omega K_{\Phi,mot}\sin(\delta_k - \omega t), \quad (2)$$

$$E_d = \varepsilon\omega K_{\Phi,EDB}\sin(2\delta_k - \omega t - \phi), \quad (3)$$

where δ_k represents the angular position of the magnetic axis of the first coil of the winding of phase *k*. The first EMF, named E_0 (2), is generated by the inductor in the windings when the rotor is centered, is independent of the out-centering amplitude and can be linked to the motor behavior of the winding. Its flux constant $K_{\Phi,mot}$ is worth $2A\left(R_{winding}\right)\sin(\frac{\tau}{2})$. The second EMF, named E_d (3), is the EMF induced by the harmonics of the magnetic field appearing when the rotor is not centered. It is proportional to the decentering amplitude, and relates to the EDB behavior of the winding. Its flux constant $K_{\Phi,EDB}$ is worth $2A^i\left(R_{winding}\right)\sin(\tau)$. From these equations, it can be seen that there will be a compromise to make on the coil pitch τ: a coil pitch of 180° maximizes the motor behavior, but cancels the EDB behavior. A coil pitch of 90° maximizes the EDB behavior, but at the expanse of a smaller flux constant related to the motor behavior.

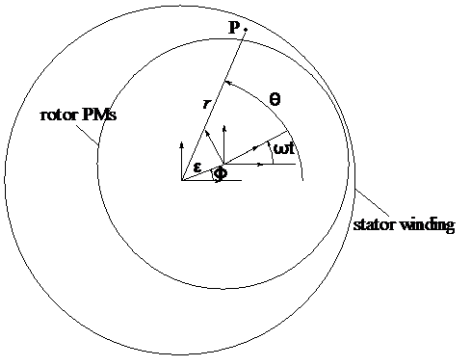

Figure 1. Frames and coordinates used for the model.

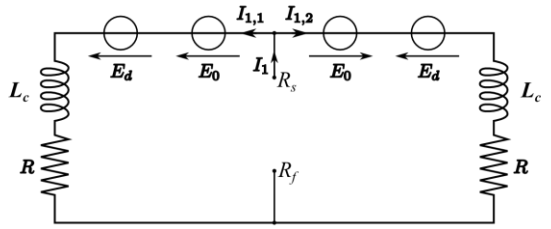

Figure 4. Equivalent electrical circuit of phase 1 of a multifunction winding for an one pole pair internal inductor, with R the resistance of one coil, L_c, the cyclic inductance of one coil, E_0 the EMF when the rotor is centered and E_d, the EMF linked to the center shift.

Equivalent electrical circuits for each phase of the multifunction winding can be represented as Fig.4, see [10]. In this circuit, the left and right branches correspond respectively to the two coils of the phase winding. Both branches have the same resistance *R*, and same cyclic inductance L_c, as both coils of the winding are identical. Two EMF appear on each part of the circuit. The motor EMF, E_0, has the same sign on both coils of the winding, given the anti-parallel connection between them. The bearing EMF, named E_d, has opposite signs for each coil given the series connection of the coils seen by the winding in this case.

The electrical equations of the equivalent circuit of phase *1*, as shown on Fig.4, are:

$$U_{R_S-R_F} + E_0 + E_d - RI_{1,1} - j\omega L_c I_{1,1} = 0 \qquad (4)$$

$$U_{R_S-R_F} + E_0 - E_d - RI_{1,2} - j\omega L_c I_{1,2} = 0 \qquad (5)$$

$$I_{1,1} + I_{1,2} = I_1 \qquad (6)$$

The same equations can be written for the *N* phases of the system.

In (6), the total current I_1 refers to the current supplied by the power supply, and it only contributes to the torque generation. Indeed, when the rotor is centered, the induced EMF E_d is equal to zero. The current distribution in each loop is then balanced and worth

$$\frac{1}{2}I_1 = I_{1,1} = I_{1,2} = \frac{U_{R_S-R_F}+E_0}{R+j\omega L_c} \qquad (7)$$

When the rotor is out-centered, an unbalance between the currents in each loop appears, generated by the EMF E_d. However, the total current I_1 remains at the same value than when the rotor is centered:

$$I_{1,1} = \frac{U_{R_S-R_F}+E_0}{R+j\omega L_c} + \frac{E_d}{R+j\omega L_c} \qquad (8)$$

$$I_{1,2} = \frac{U_{R_S-R_F}+E_0}{R+j\omega L_c} - \frac{E_d}{R+j\omega L_c} \qquad (9)$$

$$I_1 = 2\frac{U_{R_S-R_F}+E_0}{R+j\omega L_c} \qquad (10)$$

Concerning the bearing restoring forces, they can be predicted by the state-space model presented in [9], which links the two degrees of freedom point mass rotor dynamical behavior to the electrodynamic forces developed inside a heteropolar bearing. In the system analyzed in this paper, the bearing has two identical coils in series and this equation becomes:

$$\begin{bmatrix}\dot{F}\\ \ddot{z}\\ \dot{z}\end{bmatrix} = \begin{bmatrix}-\frac{R}{L_c} - j\omega_e & -\frac{2K_{\Phi,EDB}^2 N}{L_c} & -j\omega_e\left(K_d + \frac{2K_{\Phi,EDB}^2 N}{L_c}\right)\\ \frac{1}{M} & -\frac{C}{M} & 0\\ 0 & 1 & 0\end{bmatrix}\begin{bmatrix}F\\ \dot{z}\\ z\end{bmatrix}$$

In this equation, $\omega_e$is the electrical pulsation of the bearing and depends on the number of pole pairs of the rotor, and if the permanent magnets are fixed on the rotor or on the stator, *C* represents the additional damping in the system, and *M* is the rotor mass.

When the rotor is a one pole pair internal rotor, the model parameter $\omega_e$representing the electric pulsation of the rotor is worth ω.

In quasi-static conditions, i.e. when the rotor is spinning in a fixed out-centered position, these equations can be simplified, and two force components appear: one restoring component, acting to re-center the rotor, and one parasitic component, acting perpendicular to the center shift. In this case, these two components are worth:

$$F_{paral} = \frac{2N(K_{\Phi,EDB}\omega)^2 L_c}{R^2+(\omega L_c)^2}|z| \qquad (8)$$

$$F_{perp} = \frac{2N(K_{\Phi,EDB})^2 \omega R}{R^2+(\omega L_c)^2}|z| \qquad (9)$$

IV. PROTOTYPE AND TEST BENCH

A prototype of a centering heteropolar electrodynamic bearing has been constructed [11] and is now investigated for its passive self-bearing capacities, to eventually confirm the theoretical conclusions of [10], stating that in a slotless configuration, it is possible to generate sufficient passive

Figure 5. Picture of the centering heteropolar electrodynamic bearing prototype, investigated for its torque generation and self-centering capacities

electrodynamic centering forces and generate a torque in a single multifunction winding.

This prototype consists in a one pole pair permanent magnet rotor, and a 3 phase multifunction winding. The one pole pair permanent magnet is formed by an annular NdFeB permanent magnet with a parallel polarization, which allows generating a sinusoidal magnetic field inside the airgap. Each

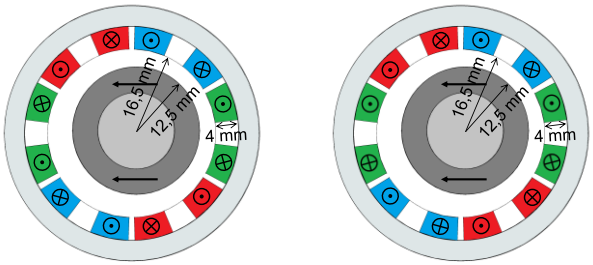

(a) (b)

Figure 6. Schematic view of the prototype, with the currents directions inside each phase resulting in (a) an electrodynamic centering force and (b) a motor torque.

phase is constituted of 2 concentrated window frame coils at 180°. There is no ferromagnetic yoke. A picture of the prototype is shown in Fig. 5, and a schematic representation of the prototype is given in Fig. 6, showing the current directions inside the windings to generate a centering force or a torque. The characteristics of the prototype are gathered in Table I.

TABLE I. CHARACTERISTICS OF THE PROTOTYPE

Parameter	Value
Outer PM rotor diameter	25 mm
Inner PM rotor diameter	15 mm
Height of PM rotor	50 mm
Rotor magnet	NdFeB
PM remanence	1.3 T
Rotor shaft	Iron
Coil turns	560
Number of coils/ phase	2
Number of phases	3
Coil wire diameter	0.2 mm
Coil total height	62 mm
Coil total width	17 mm
Coil thickness	4 mm
Stator inner diameter	33 mm
Nominal airgap	4 mm

The test bench is shown in Fig. 7. It is designed to operate in quasi-static conditions, i.e. the rotor spins in a fixed out-centered position relatively to the stator. The rotor is driven by an external motor. The stator is mounted on a xy manual stage, allowing displacing the stator with respect to the rotor with a micrometer precision. The prototype is encased inside an enclosure for safety. The test bench is also equipped with a 6-axis force sensor, measuring the reaction forces on the stator winding, and the drive torque.

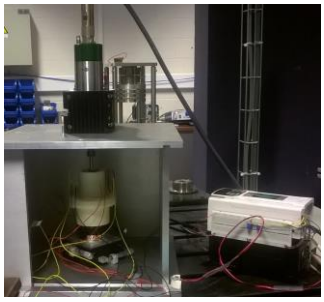

Figure 7. Picture of the test bench to operate the prototype in quasi-static conditions, with an external motor to drive the rotor.

V. ELECTROMOTIVE FORCES

A. *Experimental results*

A first experiment is carried out to characterize the electromotive forces on the windings. The windings are left in open circuit, and the 3*2 induced electromotive forces are measured on the 2 coils of the 3 phases, as shown on the equivalent circuit, in Fig. 8 for one phase.

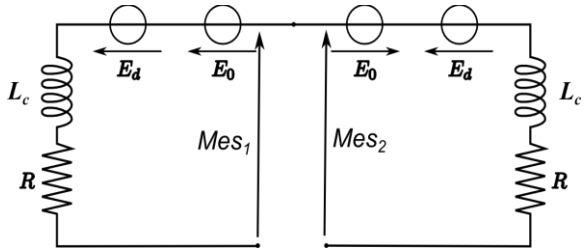

Figure 8. Principle of experimental measurements shown on equivalent electrical circuit.

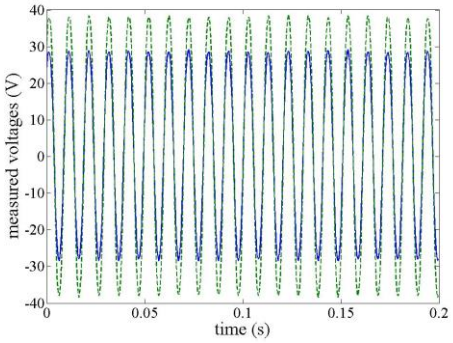

Figure 9. Measured voltages on phase 1 for a spin speed of 6000 rpm and a rotor center shift of 1.37 mm (0.6 for x-axis and 1.25 for y-axis)

This induced EMF is measured for various center shifts, and various spin speeds.

A typical example of the obtained measures is shown on Fig. 9: inside one phase, each coil undergoes signal of same frequency but, with a difference in amplitude. A Fourier

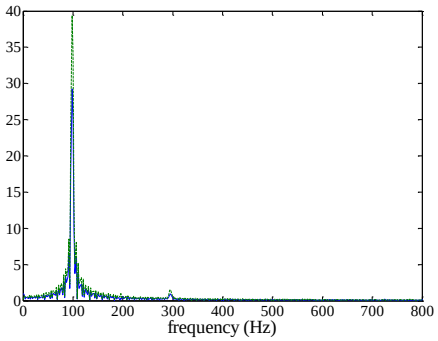

Figure 10. Fourier analysis of measured voltages shown in Fig. 9 (on phase 1 for a spin speed of 6000 rpm and a rotor center shift of 1.37 mm)

analysis of these signals is shown in Fig. 10, and confirms the same frequency of the two signals. It can also be observed that the signal is almost purely sinusoidal, although a very small third harmonic is present. This signal is post-processed to extract the first harmonic of each measure.

The amplitude of the first harmonic of these measures are illustrated in Fig. 11, for one phase, for different center shifts and spin speeds.

From these two values obtained on each phase, the electromotive force E_d, linked to the EDB, and the

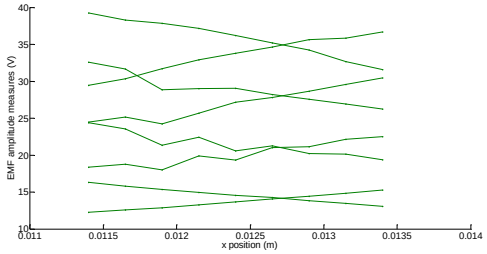

Figure 11. Amplitude of first harmonic of the measured induced voltages at the coil terminals of one phase, as a function of a rotor displacement along the x-axis, while centered along the y-axis, for rotor spin speeds of 2400, 3600, 4800 and 6000 rpm

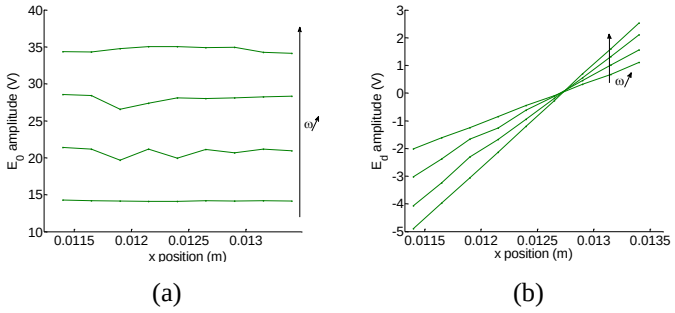

Figure 12. Amplitude of (a) motor electromotive force E_0, (b) bearing electromotive force E_d, as a function of a rotor displacement along the x-axis, while centered along the y-axis for spin speeds of 2400, 3600, 4800 and 6000 rpm

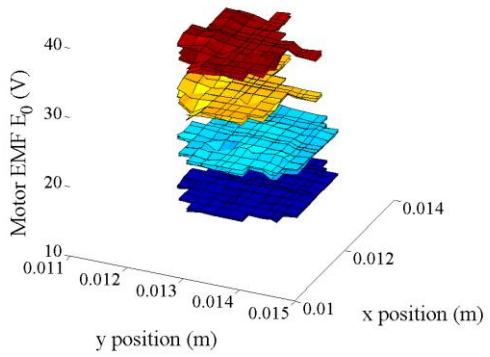

Figure 13. Motor electromotive force E_0, as a function of the rotor position in the x-y plane for spin speeds of 2400, 3600, 4800 and 6000 rpm

electromotive force E_0, linked to the motor can be deduced as shown in (8) and (9).

$$E_0 = |0.5(\overline{Mes}_1 + \overline{Mes}_2)| \qquad (10)$$

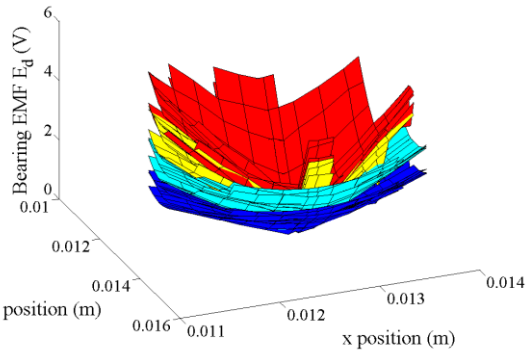

Figure 14. Amplitude of bearing electromotive force E_d, as a function of the rotor position in the x-y plane for spin speeds of 2400, 3600, 4800 and 6000 rpm

$$E_d = |0.5(\overline{Mes}_1 - \overline{Mes}_2)| \qquad (11)$$

The results at four different spin speeds for both electromotive forces, the bearing EMF E_d and the motor EMF E_0 , deduced from the measures shown in Fig. 11 based on (10) and (11), are shown in Fig. 12 (a) and (b).

These measures are carried out on the three phases, for spin

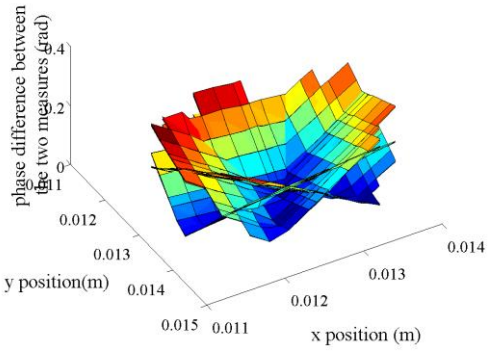

Figure 15. Phase difference between measures at the connection of one phase…

speeds of 2400, 3600, 4800 and 6000 rpm, while displacing the rotor in the x-y plane by steps of 0.25 mm, with some additional 0.1 mm steps around the rotor center. These results are shown in Fig 13 and 14. It can be observed for the motor EMF, on Fig. 13, that the induced electromotive force, only depends on the spin speed, but not on the position of the center of the rotor. The results of the measures are very similar for each phase of the prototype.

Whereas on Fig. 14, it can be observed that the bearing EMF increases proportionally with the center shift, and the slope increases with the spin speed. On the bearing EMF results, a first observation can be done on the bearing center. Indeed, due to geometric and magnetic imperfections, the geometric center of the system does not necessarily correspond to its magnetic center. The bearing EMF should be zero when the rotor is perfectly magnetically centered, and the three phases should give the same results. However, we can observe that the EMF reaches a minimum value which is situated on

slightly different (x,y) points for each phase: phase 1 (12.75,13.2) mm, phase 2 (12.65, 13.2) mm, and phase 3 (12.75, 13.2) mm. This illustrates that there is a slight dissymmetry between the phases. By displacing the rotor center by steps of 0.25 mm or 0.1 mm, the exact magnetic center is not found and the bearing EMF minimum value is a little bit higher than zero: 0.2 V for the highest value at 6000 rpm. It can also be seen in Fig. 14 that those small differences between the phases remain for all the measured points, compared to 5.7 V for the highest spin speed and the highest center shift considered for the measures.

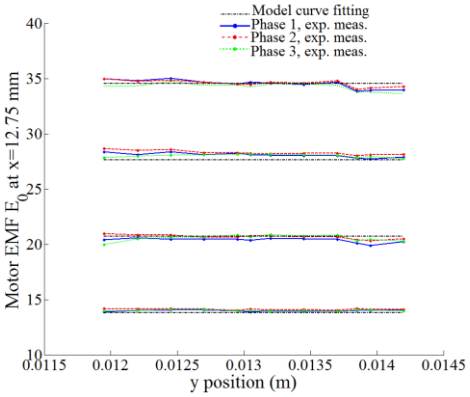

Figure 16. Motor electromotive force E_0 amplitude, as a function of a rotor displacement along the y-axis, while centered along the x-axis for spin speeds of 2400, 3600, 4800 and 6000 rpm. Measures for the three phases, and model curve fitting predictions

Fig. 15, also shows that there is a phase shift between the two measures, on the left and right coil of each phase. This phase shift reflects the direction of the center shift, and between each phase there is a phase shift of 120°.

B. EMF experimental- model comparisons

The model predicts a bearing EMF proportional to the spin speed and to the center shift (3), and a motor EMF only proportional to the spin speed (2). This is indeed observed on Fig. 13 and 14, and is even easier to observe in 2D Fig.16 and 17. On these figures the rotor is centered along the x-axis, by placing the rotor at the x-position giving minimum bearing EMF value, x=12.75 mm. Measures are carried out for different y-axis rotor positions. The bearing and motor EMF are also predicted by the model, thanks to (2) and (3). The flux constants $K_{\Phi,mot}$ and $K_{\Phi,EDB}$ are calculated by FE simulations or by performing a curve fitting on the experimental measures, using a least square criterion. The numerical values, obtained in the two cases, for these flux constants are given in Table 2. The measures for the three phases and the model predictions are represented in Fig. 16, for the motor EMF, and on Fig. 17 for the bearing EMF.

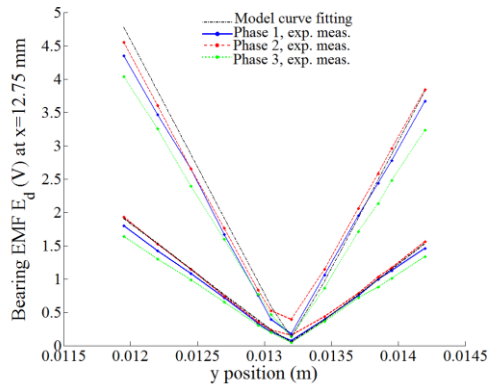

Figure 17. Bearing electromotive force E_d amplitude, as a function of a rotor displacement along the y-axis, while centered along the x-axis for spin speeds of 2400, 3600, 4800 and 6000 rpm. Measures for the three phases, and model curve fitting predictions

TABLE II. EMF MODEL PARAMETER IDENTIFICATION

Parameter	FE Value	Exp. Curve fitting value	Relative difference
$K_{\Phi,mot}$	0.0473	0.0389	21.6%
$K_{\Phi,EDB}$	4.3027	4.1366	4.9%

VI. FORCE AND TORQUE

A second experiment is carried out, by connecting the two coils of each phase in series, and by driving the rotor by the external motor. The motor is thus analyzed in a generator mode. In these conditions, a first set of measures on the restoring radial forces and the drag torque is done by leaving the motor connections of each phase are in open circuit. A second set of measures is done by connecting a resistive charge on the motor connections and by measuring again the radial forces and the resistive torque.

A. Bearing forces

Referring to (8) and (9), the electrodynamic bearing forces are proportional to the center shift. This is indeed observed on Fig. 18 and 19, where the centering and perpendicular force, as a function of the rotor displacement along the x-axis, while centered along the y-axis is shown for a spin speed of 6000 rpm. The measures when the generator is left in open circuit, and when it is connected to a 200 Ω charge, are similar, and

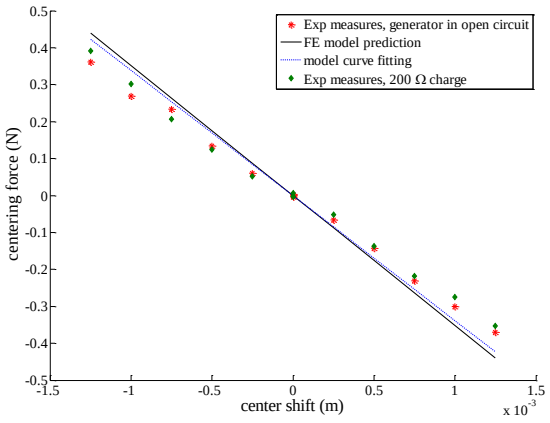

Figure 18. Bearing restoring force, as a function of the rotor displacement along the x-axis, while centered along the y-axis for a spin speeds of 6000 rpm. Measures when the generator is left in open circuit, and when connected to a 200 Ω charge, and comparison to the model when its parameters are identified by FE simulations, and by curve fitting

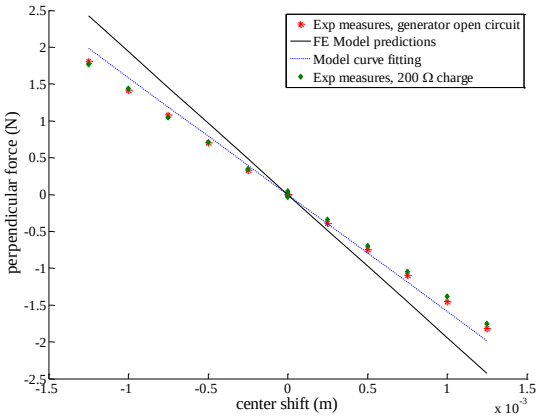

Figure 19. Bearing force perpendicular to the center shift, as a function of the rotor displacement along the x-axis, while centered along the y-axis for a spin speeds of 6000 rpm. Measures when the generator is left in open circuit, and when connected to a 200 Ω charge, and comparison to the model when its parameters are identified by FE simulations, and by curve fitting

show that the bearing forces are not influenced by the generator behavior at that spin speed. The comparison with the model predictions when its parameters are identified either by FE simulations, either by curve fitting, is also shown, and there is a good correspondence. The value of the model parameters is given in Table 3.

TABLE III. FORCE MODEL PARAMETER IDENTIFICATION

Parameter	FE Value	Exp. Measure	Curve fitting
$R \ (\Omega)$	44.11	42.08	42.1
$L_c(H)$	0.0127	0.0162	0.0143

The stiffness reached by the recentering force at 6000 rpm is worth 297.4 N/m, which is very low. However, the spin speed remains low, and the electrodynamic stiffness developed by electrodynamic bearings increases with the spin speed. It can also be observed on these figures that at the spin speed of 6000 rpm, the parasitic force, perpendicular to the center shift is more important than the restoring force.

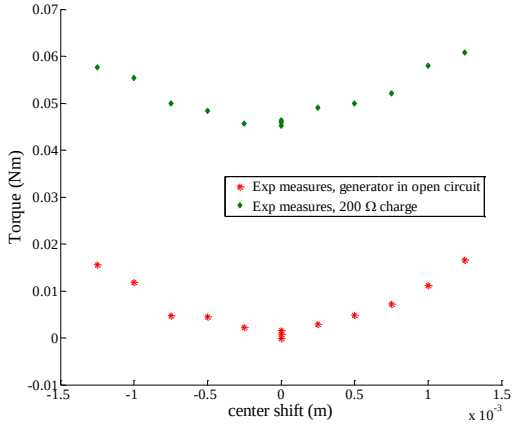

Figure 21. Measured torque, as a function of the rotor displacement along the x-axis, while centered along the y-axis for a spin speed of 6000 rpm. Measures when the generator is left in open circuit, and when connected to a 200 Ω charge.

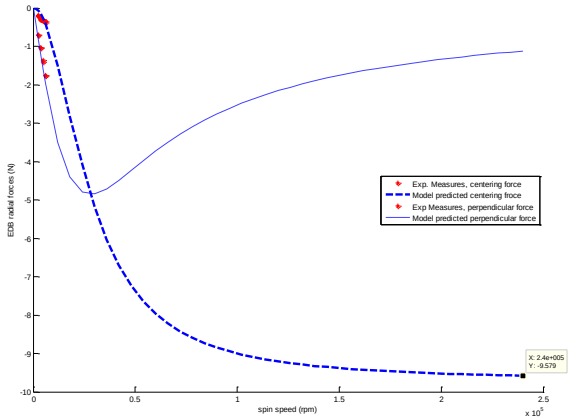

Figure 20. Bearing forces as a function of the spin speed, for a center shift of 1.25 mm

This is due to the fact that, at 6000 rpm, the rotor is not spinning fast enough in comparison to the electrical pole. The restoring force becomes more important when the spin speed becomes higher than the electrical pole of the system [6]. The model predictions for this bearing show that when extrapolating at higher spin speed, the perpendicular force decreases, and the restoring stiffness increases up to 7660 N/m, see Fig. 20.

An additional word should be said on the well-known dynamical stability problems of centering electrodynamic bearings: the force perpendicular to the center shift will produce dynamical instability, and the system needs some damping in order to be stable dynamically when spinning. The dynamics of such a system are studied in detail through root locii in [9] for heteroplar electrodynamic bearings: they will depend on the R-L dynamics of the bearing winding and on the mechanical time constant of the system. As all the measures presented in this article were performed in quasi-static, these instabilities do not appear.

B. Torque

The torque is also measured for the two cases: with the

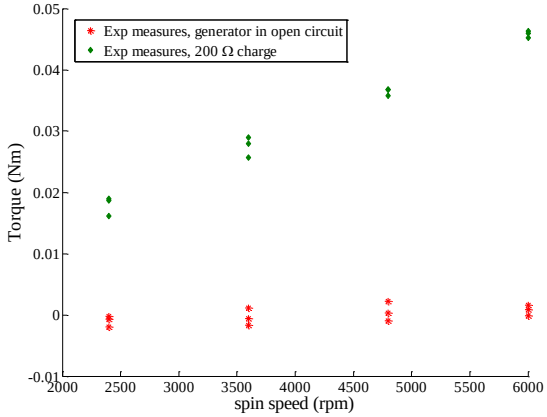

Figure 22. Measured torque, as a function of the spin speed, when the rotor is centered. Measures when the generator is left in open circuit, and when connected to a 200 Ω charge.

generator in open circuit and with a resistive charge connected to its terminals. It can be observed on Fig. 21, that when there is no charge on the motor terminal, there is a torque measured, which corresponds to the electrodynamic drag torque. This torque increases when the center shift increases. When the resistive charge is connected, an additional torque appears, corresponding to the motor torque. This motor torque is proportional to the spin speed, as can be seen in Fig. 22, and remains constant while off-centering the rotor. In this figure, it can also be observed that when the rotor remains centered, the electrodynamic torque remains around zero, which confirms the null-flux principle: when the electrodynamic bearing is magnetically centered, there is no power dissipated inside the windings due to its bearing function, and no forces generated.

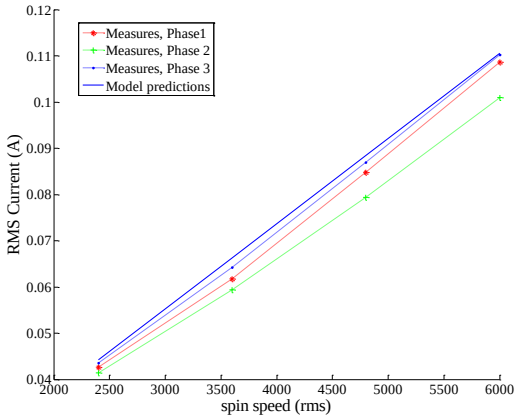

Figure 23. Model predicted and measured RMS current inside the resistive charge, as a function of the spin speed, when the rotor is centered, and the generator connected to a 200 Ω charge.

Finally, the current flowing through the resistive charge has also been measured, and is shown in Fig. 23, for the three phases. It corresponds to the current predicted by solving the electrical circuit of Fig 4, with a resistive charge at the terminals R_S-R_F. The maximum measured current, at the max center shift (1.25 mm) and the maximum spin speed (6000 rpm) is worth 0.119 A-rms. This corresponds to a current density of 3.79 A/mm². This means that a higher spin speed or a lower resistive charge could be considered on this prototype without risk to damage the coils.

However, even with these conditions, the produced torque and reached stiffness are low, which can be explained by the fact that this prototype was designed to be a bearing only intended to demonstrate the null-flux principle in heteropolar EDB, without optimization of its performances in the sizing process.

VII. CONCLUSION

This paper shows experimental measures made on a heteropolar electrodynamic bearing to evaluate its performance to operate as a passively centered self-bearing permanent magnet rotor. First the operating principle is briefly explained. Second, EMF measurements show a motor EMF independent from the rotor center position and a bearing EMF proportional to the rotor displacement. Third, torque and force measurements show radial forces measurements in agreement with electrodynamic centering bearing forces, presenting a restoring component and a component perpendicular to the center shift. The torque measurements show an electrodynamic drag torque depending on the rotor position, and a motor torque proportional to the spin speed. Although a low produced torque and reached stiffness, these experimental measures confirm the feasibility of the operating principle for a slotless winding without ferromagnetic yoke and a permanent magnet rotor, supposing that there is enough damping in the system to counter the dynamical instabilities inherent to centering electrodynamical bearings.

REFERENCES

[1] A. Chiba, T. Fukao, M. A. Rahman, "Vibration Suppression of a Flexible Shaft with a Simplified Bearingless Induction Motor Drive," *Industry Applications Conference, 41st IAS Annual Meeting. Conference Record of the 2006 IEEE*, vol. 2, pp 836-842, 2006.

[2] A. Laiho, A. Sinervo, J. Orivuori, K. Tammi, A. Arkkio, K. Zenger,"Attenuation of harmonic rotor vibration in a cage rotor induction machine by a self-bearing force actuator," *IEEE Trans. on Magnetics*, vol. 45(12), pp5388-5398, 2009.

[3] C. Xin, D. Zhiquan, W. Xiaolin, "Vibration Reduction with Radial Force Windings Short-circuited in Bearingless Switched Reluctance Motors," *4th IEEE Conference on Industrial Electronics and Applications*, pp.2630-2634, 2009.

[4] V. Kluyskens and B. Dehez, "Dynamical electromechanical model formagnetic bearings subject to eddy currents," IEEE Trans. Magn., vol. 49(4), pp. 1444–1452, Apr. 2013

[5] J. G. Detoni, "Progress on electrodynamic passive magnetic bearings for rotor levitation," Proc. Inst. Mech. Eng. C, J. Mech. Eng. Sci., vol. 228, no. 10, pp. 1829–1844, Jul. 2014

[6] N. Amati, X. De Lépine, A. Tonoli, "Modeling of Electrodynamic Bearings," Journal of Vibraitons and Acoustics, Vol. 130, pp061007-1-9, Dec. 2008.

[7] A.V. Filatov and E. H. Maslen, "Passive Magnetic Bearing for Flywheel Energy Storage Systems," IEEE Trans Magn., vol. 37(6), pp 3913-3923, Nov 2001

[8] C. Dumont, V. Kluyskens, B. Dehez "Null-flux radial electrodynamic bearing", *IEEE Trans. on Magnetics*, vol. 50(10), 8102212 , 2014.

[9] C. Dumont, V. Kluyskens, and B. Dehez, "Linear state-space representation of heteropolar electrodynamic bearings with radial magnetic field," IEEE Trans. Magn., vol. 52(1), 8100109, Jan. 2016.

[10] V. Kluyskens, C. Dumont, B. Dehez, "Description of an Electrodynamic Self-Bearing Permanent Magnet Machine", *IEEE Trans. on Magnetics*, vol 53(1), 8100409, 2016

[11] C. Dumont, V. Kluyskens, B. Dehez, "Design and experimental testing of a heteropolar electrodynamic bearing", 2nd IEEE Conference on Advances in Magnetics, La Thuile, Italy, 4-7 February 2018.